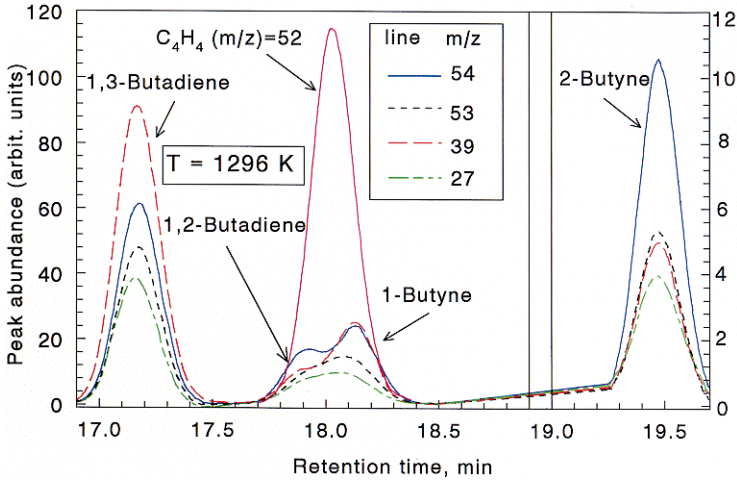

FIGURE 16.4.5 GC-MS chromatogram using the single-ion monitoring mode of the mass selective detector. Peaks of 1,2-butadiene and 1-butyne are hidden behind a large peak of C_4H_4 and can be analyzed only with the assistance of the GC-MS.

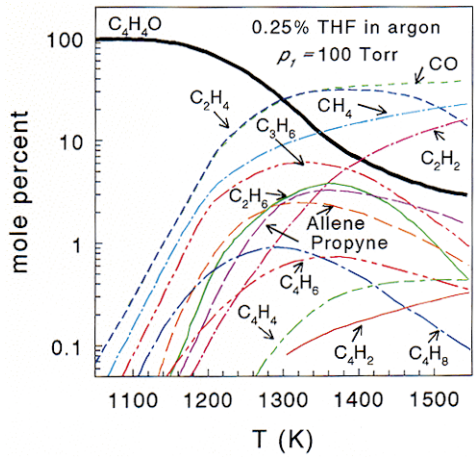

FIGURE 16.4.6 Product distribution in the decomposition of shock-heated tetrahydrofuran.

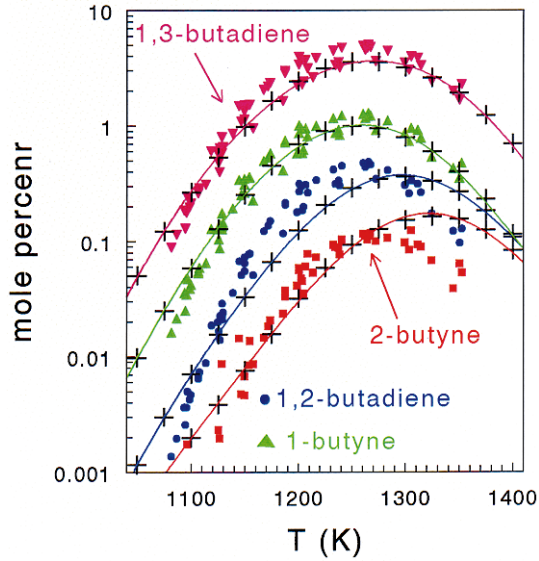

FIGURE 16.4.17 Experimental and calculated mole percents of the four isomers of C_4H_6. The points are the experimental values and the lines are the best fit through the calculated points shown here as crosses.

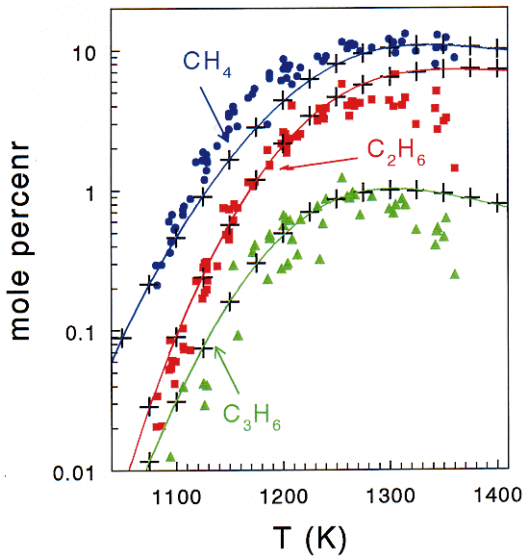

FIGURE 16.4.18 Experimental and calculated mole percents of methane, ethane, and propylene. The symbols are the experimental points and the lines are the best fit through the calculated points shown here as crosses.

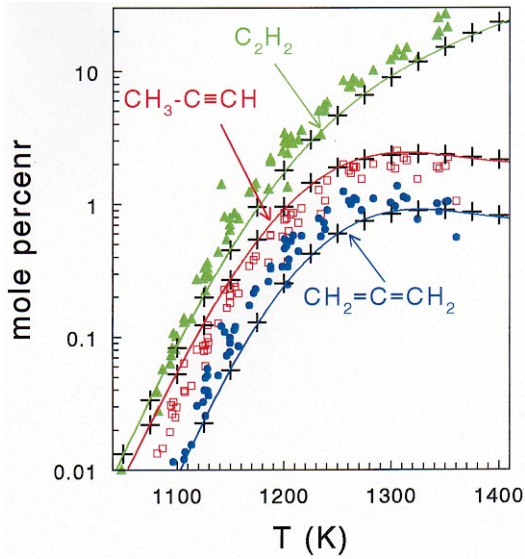

FIGURE 16.4.20 Experimental and calculated mole percents of allene, propyne, and acetylene. The symbols are the experimental points and the lines are the best fit through the calculated points shown here as crosses.

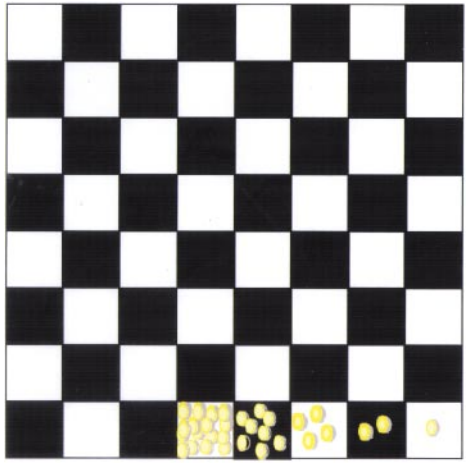

FIGURE 16.5.1 Wheat grains arranged on a chessboard in a geometrical series

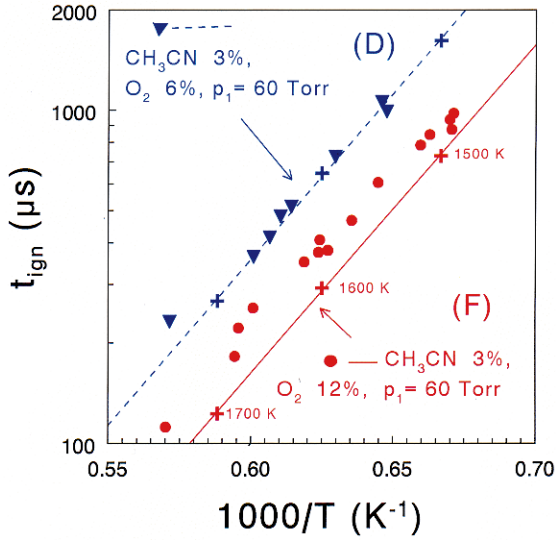

FIGURE 16.5.4 Experimental (points) and calculated (lines) ignition delays in two different mixtures of $CH_3CN + O_2$ in argon. From the distance between the two series of experiments, the power dependence with respect to oxygen, $\beta_{(O_2)}$, can be determined. A strong enhancing effect of oxygen can be seen

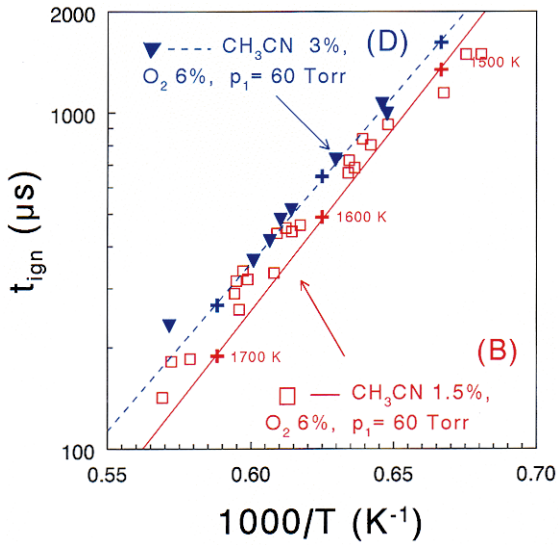

FIGURE 16.5.5 Experimental (points) and calculated (lines) ignition delays in two different mixtures of $CH_3CN + O_2$ in argon. From the distance between the two series of experiments, the power dependence with respect to the fuel, $\beta_{(CH_3CN)}$, can be determined. A small inhibiting effect of acetonitrile can be seen

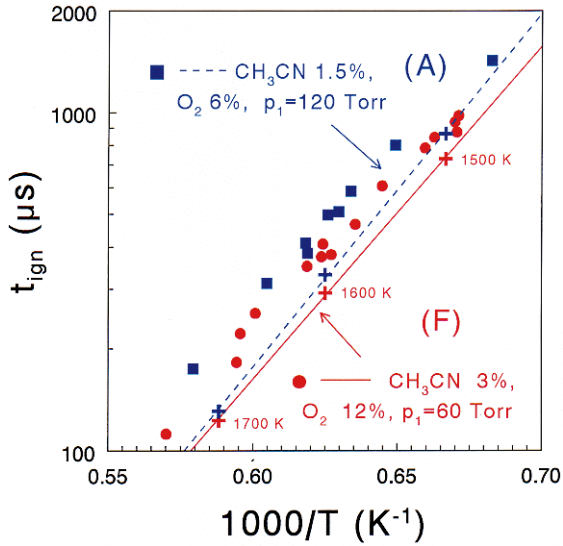

FIGURE 16.5.6 Experimental (points) and calculated (lines) of ignition delays in two different mixtures of $CH_3CN + O_2$ in argon. From the distance between the two series of experiments, the power dependence with respect to the diluent argon, $\beta_{(Ar)}$, can be determined. A very small inhibiting effect of argon can be seen

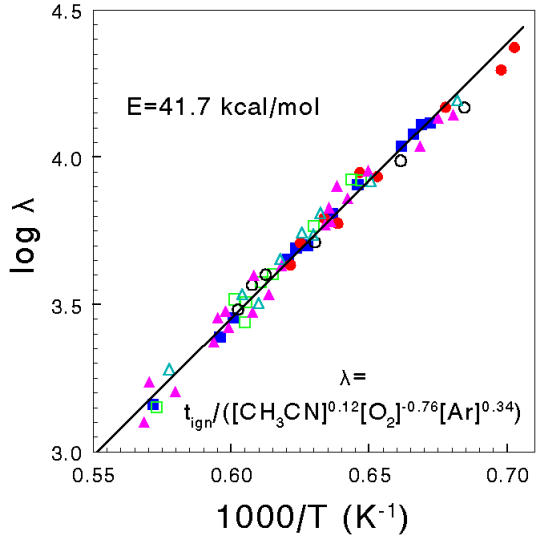

FIGURE 16.5.7 A plot of $\log \lambda$ vs $1/T$, where $\lambda = t_{\text{ignition}}/\{[CH_3CN]^{0.12}, [O_2]^{-0.76}, [Ar]^{0.34}\}$ for data points from six series of experiments. With the above correlation, all the points scatter along one line with a slope of 41.7 kcal/mol

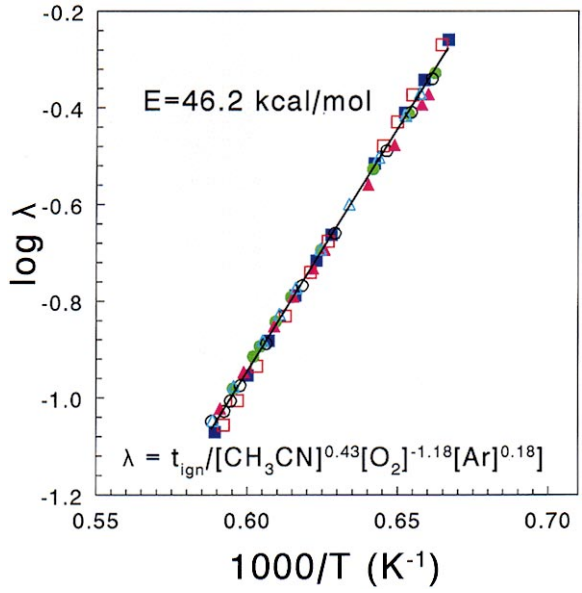

FIGURE 16.5.13 A plot of $\log \lambda$ vs $1/T$ where $\lambda = t_{\text{ignition}}/\{[CH_3CN]^{0.43}, [O_2]^{-1.18}, [Ar]^{0.18}\}$ for 60 calculated points corresponding to the six series used in the experiments. With the above correlation, all the calculated points scatter along one line with a slope of 46.2 kcal/mol

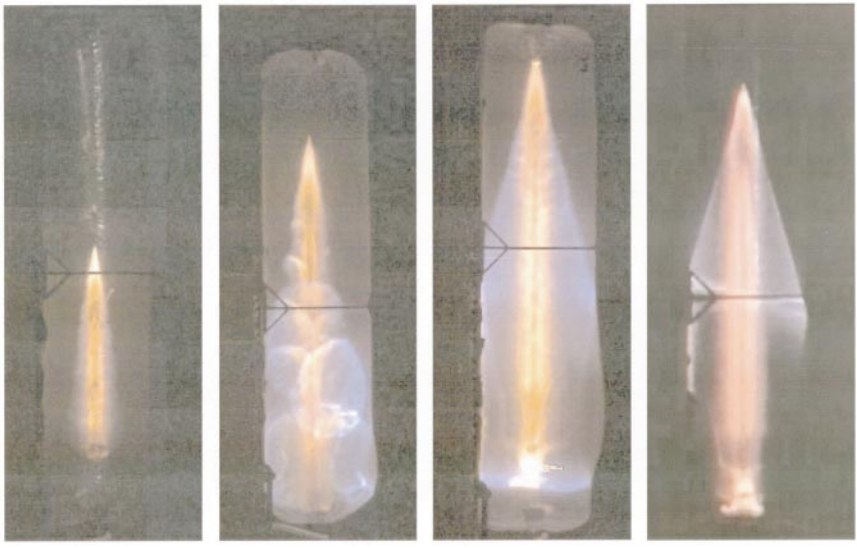

FIGURE 17.20 Regimes of cylindrical blast initiation in C_2H_4–air mixture by a PETN detonation cord: (a) supercritical, (b, c) critical, (d) subcritical.